J Solid State Electrochem (2014) 18:2841–2846
DOI 10.1007/s10008-014-2543-7

ORIGINAL PAPER

Facile synthesis of multiwalled carbon nanotube–V_2O_5 nanocomposites as cathode materials for Li-ion batteries

Mulan Qin · Jun Liu · Shuquan Liang · Qing Zhang · Xilin Li · Yue Liu · Meiying Lin

Received: 21 March 2014 / Revised: 7 June 2014 / Accepted: 15 June 2014 / Published online: 28 June 2014

Abstract Multiwalled carbon nanotube (MWCNT)–vanadium pentoxide (V_2O_5) nanocomposites have been fabricated using a facile and environmental friendly hydrothermal method without any pretreatment, surfactants, or chelate agents added. The as-annealed nanocomposites are characterized by X-ray diffraction (XRD), scanning electron microscopy (SEM), and transmission electron microscopy (TEM), and the results indicate that V_2O_5 nanoparticles grew on MWCNTs. As a cathode material for lithium batteries, it exhibits superior electrochemical performance compare to the pure V_2O_5 powders. A high specific discharge capacity of 253 mA h g^{-1} can be obtained for the 15 % MWCNT–V_2O_5 nanocomposite electrodes, which retains 209 mA h g^{-1} after 50 cycles. However, the pure V_2O_5 powder electrodes only possess a specific discharge capacity of 157 mA h g^{-1} with a capacity retention of 127 mA h g^{-1} after 50 cycles. Moreover, the MWCNT–V_2O_5 nanocomposite electrodes show an excellent rate capability with a specific discharge capacity of 180 mA h g^{-1} at the current rate of 4 C. The enhanced electrochemical performance of the nanocomposites is attributed to the formation of conductive networks by MWCNTs, and large surface areas of V_2O_5 nanoparticles grew on MWCNTs which stabilizes these nanoparticles against agglomeration.

Keywords Vanadium pentoxide · Nanocomposite · Multiwalled carbon nanotube · Cyclic performance · Cathode

M. Qin · J. Liu (✉) · S. Liang (✉) · X. Li · Y. Liu · M. Lin
Department of Materials Science and Engineering, Central South University, Changsha, Hunan 410083, China
e-mail: liujun4982004@csu.edu.cn
e-mail: lsq@mail.csu.edu.cn

Q. Zhang
Department of Chemistry and Chemical Engineering, Central South University, Changsha, Hunan 410083, China

Introduction

Lithium-ion batteries (LIBs) have been widely used in portable electronic devices, such as laptops and cell phones mainly due to their high energy density and good cycle performance [1, 2]. However, their relatively low charge/discharge rates have limited their use in applications that require both high power and high capacity, such as hybrid electric vehicles (HEVs) and electric vehicles (EVs). Developing new electrode materials with much higher electrochemical performance than conventional materials has become an urgent demand to meet the increasing requirements to the new technologies and industries.

Vanadium pentoxide (V_2O_5), due to its high energy densities, abundant source, low cost, and easy synthesis, is considered to be one of the attractive candidate cathode materials for LIBs [3]. However, the intrinsic poor diffusion coefficient of lithium ions (10^{-12} to 10^{-15} cm^2 s^{-1}) [4] and low electronic conductivity (10^{-2} to 10^{-3} S cm^{-1}) [5] in crystalline V_2O_5 hinder the practical widespread utilization of this material as a cathode in LIBs. Nanostructured vanadium pentoxide has demonstrated much improved lithium-ion intercalation properties by shorting diffusion distance for both lithium ions and electrons, and the specific power can be improved due to a much increased surface area for intercalation–deintercalation reactions of lithium ions [5, 6]. Various nanostructured vanadium pentoxides, such as nanorods [7, 8], nanofibers [9, 10], nanobelts [11, 12], nanowires [13], nanotubes [14], and microporous structures [15, 16], have been synthesized using different methods, including template-based electrodeposition methods [7, 14], electrospinning method [9], reverse micelle techniques [10], hydrothermal synthesis [11, 12], solvothermal method [16], thermal evaporation [8], and hydrolysis method [17]. The low electronic conductivity of V_2O_5 is another key reason that limited its applications as an electrode material.

Carbon nanotubes (CNTs), because of their unique one-dimensional tubular structure, large surface area, high electrical conductivity, and electrochemical stability, have been considered an ideal nanomaterial to functionalize other materials for applications in energy conversion and storage [18]. Composites of V_2O_5 or hydrous V_2O_5 mixed with CNTs have good performance at high discharge rates. Dunn's group [19] incorporated V_2O_5 aerogels into single-walled carbon nanotubes (SWNTs) using a sol–gel method, and the nanocomposite electrode shows high capacities exceeding 400 mA h g^{-1} at high rates. Sathiya et al. [20] coated the functional multiwalled carbon nanotubes with a thin layer of V_2O_5 aerogels by controlled hydrolysis of vanadium alkoxide and got enhanced electrochemical performance. Hu et al. [21] prepared V_2O_5/carbon tube-in-tube material (CTIT) nanocomposite using the incipient wetness impregnation method, which owned good lithium permeation and electrochemical stability. Seng's group [22] prepared multiwalled carbon nanotubes (MWCNTs)/V_2O_5 nanocomposite by adding the MWCNTs to V_2O_5 nanowire dispersion with ultrasonic treatment, which showed good rate capability and recyclability. Chen et al. [23] coated a multiwalled carbon nanotube sponge network by atomic layer deposition (ALD) V_2O_5, and the composite showed high areal capacity and power density as Li-ion cathodes. Cao and Wei [24] synthesized V_2O_5 nanoparticle/SWNT mesoporous hybrid films with high-rate capacities using a floating CVD method followed by controllably hydrolytic deposition of V_2O_5 nanoparticles. Such nanocomposites provide favorable diffusion pathways for both electrons and lithium ions, which are essential for high-rate rechargeable lithium-ion batteries. However, the synthesis of these composites is more complicated.

Herein, we report a facile and environmental friendly hydrothermal method without any pretreatment, surfactants, or chelate agents added to fabricate a hybrid nanomaterial consisting of V_2O_5 nanocrystals and MWCNTs. Compared to synthesized pure V_2O_5 powders, MWCNT–V_2O_5 nanocomposites showed much improved electrochemical performances as a cathode material for LIBs.

Experimental

Synthesis of MWCNT–V_2O_5 nanocomposites

All the reagents and solvent were used without further purification. The MWCNT–V_2O_5 nanocomposites were synthesized by a facile hydrothermal approach. In a typical process, 0.364 g of commercial V_2O_5 was dispersed into 20 mL of distilled water, and then, 5 mL of 30 % H_2O_2 was added to the above solution under vigorous stirring and kept for 1 h at room temperature. At the same time, 0.0546 g (15 wt% of V_2O_5) of as-received MWCNTs was dispersed into 10 mL of distilled water under ultrasonication. Finally, the above two solutions were mixed and the mixture was stirred for another 1 h to form a homogenous dispersion. The dispersion was transferred to a 40-mL Teflon-lined stainless steel autoclave and kept in an oven at 200 °C for 4 h and then allowed to cool to ambient temperature. The product was washed with distilled water and ethanol for several times and was firstly dried at 60 °C overnight and then dried in a vacuum oven at 100 °C for 10 h to yield the precursor. Finally, the produced precursor was calcined at 400 °C for 1 h in air to obtain the nanocomposites. For comparison, pure V_2O_5 powders were also obtained using a similar process as described above in the absence of MWCNTs. MWCNTs were supplied by Nanjing XFNANO Materials Tech Co., Ltd., the diameter is 50 nm, and the length ranged from 10 to 30 μm.

Characterization

The phase structures of the synthesized pure V_2O_5 powders and MWCNT–V_2O_5 nanocomposites were determined by X-ray diffraction (XRD) (Rigaku D/max2500 XRD with Cu Kα radiation, λ=1.54178 Å). A scanning electron microscope (SEM) (FEI Sirion200) and a field emission transmission electron microscope (FETEM) (JEOL JEM-2100 F) were used to characterize the structural morphologies of the synthesized products.

The electrochemical performance of the as-prepared powders was investigated using two-electrode coin-type cells (CR 2016) with lithium foil as a reference electrode. MWCNT–V_2O_5 nanocomposites or pure V_2O_5 powders, acetylene black, and polyvinylidene fluoride (PVDF) binder in a weight ratio of 8:1:1 were mixed and then dispersed in an *N*-methyl-2-pyrrolidone (NMP) solution to make a slurry. The slurry was coated on aluminum foil and dried in a vacuum oven at 90 °C for 20 h prior to coin cell assembly. The cells (2016-type coin cells) were assembled in a glove box (MBraun, Germany) filled with ultrahigh purity argon, using polypropylene membrane as the separator and 1 M $LiPF_6$ dissolved in ethylene carbonate/dimethyl carbonate (EC/DMC) at a volume ratio of 1:1 as the electrolyte. Cyclic voltammetry and electrochemical impedance measurements were performed with a CHI660c and an IM6ex electrochemical workstation, respectively. The galvanostatic charge–discharge characteristics of the cells were recorded with a land battery tester (Land CT2001A; Wuhan, China) in the voltage range of 2.05–4.0 V (versus Li/Li^+) at room temperature. The specific capacity of the MWCNT–V_2O_5 nanocomposites was calculated by using the total mass of V_2O_5+MWCNTs.

Results and discussion

Structure and morphology

The X-ray diffraction patterns of pure V_2O_5 powders and 15 % MWCNT–V_2O_5 nanocomposites are presented in Fig. 1. As shown in Fig. 1, the XRD peaks for the synthesized samples are all indexed and can be well assigned to the orthorhombic structure of V_2O_5 with the *Pmmn* space group (JCPDS Card No. 41-1426, a=11.519, b=3.564, c=4.374). No impurity is found in the products as there are no other miscellaneous peaks being detected. For the nanocomposites, the characteristic peak at $2\theta=26.2°$ arising from the MWCNTs [18] was coincided with (110) of orthorhombic V_2O_5. However, the intensity of the peaks for the nanocomposites is weaker and the breadth is much wider, which suggests worse crystallinity and much smaller grain size.

Figure 2 shows the morphologies of synthesized V_2O_5 powders and MWCNT–V_2O_5 nanocomposites. The pure V_2O_5 powders consist of bulk with the size in the micro range. The nanocomposite contains MWCNTs that are mixed with V_2O_5 nanoparticles. With the increasing of content of MWCNTs, the V_2O_5 nanoparticles grown on the MWCNTs have smaller dimensions. The transmission electron microscope (TEM) images (Fig. 3) further reveal that the surfaces of the MWCNTs are coated with a layer of V_2O_5 nanoparticles. As the V_2O_5 nanoparticles grow directly on the surface of MWCNTs, not just mixed simply with MWCNTs, it is believed that the excellent interaction of V_2O_5 nanoparticles and MWCNTs should result in improved electrochemical performance.

Electrochemical performance

The electrochemical properties of the cathode materials were evaluated using 2016-type coin cells. Figure 4a shows the discharge curves of the second cycles of the synthesized pure

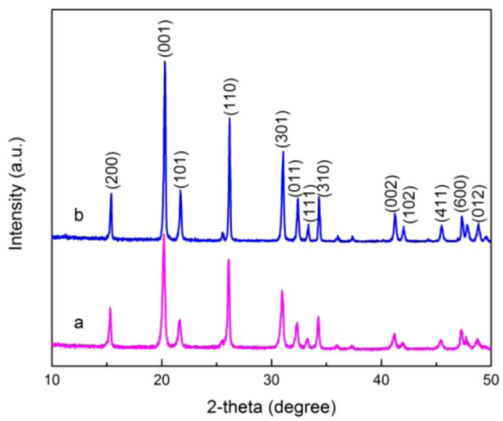

Fig. 1 XRD patterns of samples prepared by hydrothermal method **a** with MWCNTs and **b** without MWCNTs

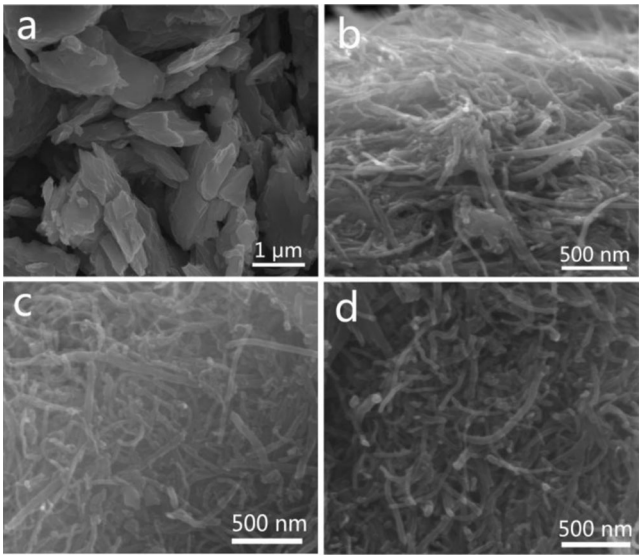

Fig. 2 SEM images of **a** V_2O_5 powders, **b** 5 % MWCNT–V_2O_5 nanocomposites, **c** 10 % MWCNT–V_2O_5 nanocomposites, and **d** 15 % MWCNT–V_2O_5 nanocomposites

V_2O_5 powders and MWCNT–V_2O_5 nanocomposites. No obvious plateaus during discharge were observed in the voltage range between 4.0 and 2.05 V for the V_2O_5 powder electrode, and a specific discharge capacity of 157 mA h g^{-1} is obtained in this voltage range at a current density of 50 mA g^{-1}. However, the MWCNT–V_2O_5 nanocomposite electrode has three obvious plateaus and the higher specific discharge capacity is obtained, with 253, 274, and 228 mA h g^{-1} for 15, 10, and 5 % MWCNT–V_2O_5 nanocomposites, respectively. Figure 4b compares the cyclic performance of the V_2O_5 powders and MWCNT–V_2O_5 nanocomposites at a current density of 50 mA g^{-1} at room temperature. Fifteen percent MWCNT–V_2O_5 nanocomposite electrode delivers an initial specific discharge capacity of 243 mA h g^{-1}, and its capacity retained to be 209 mA h g^{-1} at 50 cycles. By contrast, the V_2O_5 powder electrode delivers a much lower initial discharge capacity of 155 mA h g^{-1}, and the capacity then drops to 127 mA h g^{-1} at 50 cycles. As a higher electronic conductivity of V_2O_5 electrodes corresponds to a higher cycle performance [19, 22], the improved cyclic performance of the MWCNT–V_2O_5 electrodes was mainly attributed to the excellent electrical conductivity of MWCNTs and the

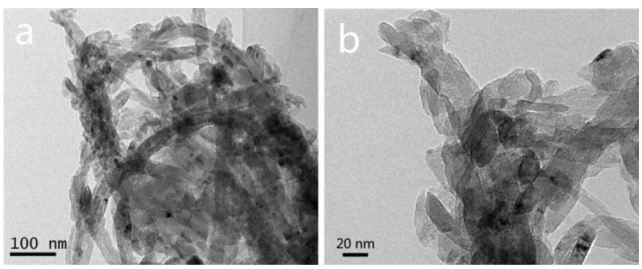

Fig. 3 TEM photographs of 15 % MWCNT–V_2O_5 nanocomposites

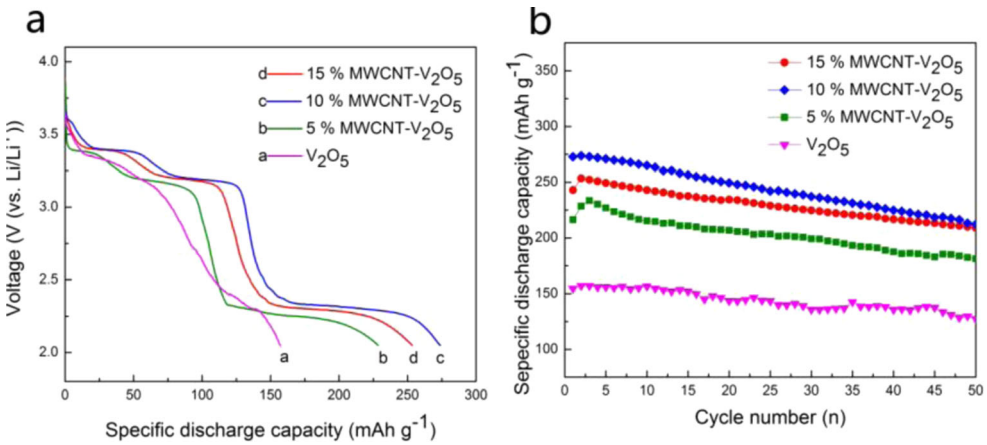

Fig. 4 **a** Galvanostatic discharge curves of samples and **b** residual discharge capacity vs. the cycle number at the current density of 50 mA g^{-1}

hybridization with the active material. It is found that 15 % MWCNT–V_2O_5 nanocomposites have a lower initial discharge capacity than 10 % MWCNT–V_2O_5 nanocomposites, which is due to the fact that there is less actual content of V_2O_5-active material in 15 % MWCNT–V_2O_5 nanocomposites. With the increasing of MWCNTs content, the nanocomposites have better cycle performance as there are more electrical conductivity and smaller V_2O_5 nanoparticles sizes.

Figure 5 reveals cyclic voltammogram curves for both V_2O_5 powders and 15 % MWCNT–V_2O_5 nanocomposites at a scan rate of 0.1 mV s^{-1}. It can be seen that the peak positions shown on the CV curves correspond well with the charge/discharge plateaus. The observation of three main peaks at 3.36, 3.15, and 2.21 V during the cathodic scan indicates the multistep lithium-ion intercalation process, and the phases change from α-V_2O_5 to ε-$Li_{0.5}V_2O_5$ (3.36 V), δ-LiV_2O_5 (3.15 V), and γ-$Li_2V_2O_5$ (2.21 V), consecutively [25, 26]. In the anodic scan, three peaks at 2.59, 3.26, and 3.46 V vs. Li/Li^+ are observed, which correspond to the removal of the Li^+ [27, 28]. For comparison, the CV curve of pure V_2O_5 electrode is also shown in Fig. 5. Only two broad peaks around 3.04 and 3.92 V vs. Li/Li^+ are detected during the deintercalation process. Comparing the two curves of different samples, it is apparent that the 15 % MWCNT–V_2O_5 nanocomposite electrode has less polarization, which is attributed to the reduced particle size. Another distinguishing feature is that the peak current density of 15 % MWCNT–V_2O_5 nanocomposites was much larger than that of pure V_2O_5 powders. It has been reported that if the charge transfer at the interface is fast enough and the rate-limiting step is the lithium diffusion in electrode, then the peak current is proportional to the contact area between the electrode and the electrolyte [8, 29, 30]. The higher contact surface area between electrode material and electrolyte for MWCNT–V_2O_5 nanocomposite electrode certainly increases the peak current density. This observation is evident to kinetic reversibility of lithium-ion intercalation into and extraction from the V_2O_5 nanoparticles and the significantly improved electrochemical performance of MWCNT–V_2O_5 nanocomposites.

The electrochemical impedance spectra (EIS) of V_2O_5 powders and MWCNT–V_2O_5 nanocomposites are shown in Fig. 6. The date was collected with a two-electrode coin cell in the frequency range from 100 kHz to 0.01 Hz at 3.4 V after 3 cycles. The Nyquist plots are typically represented by two

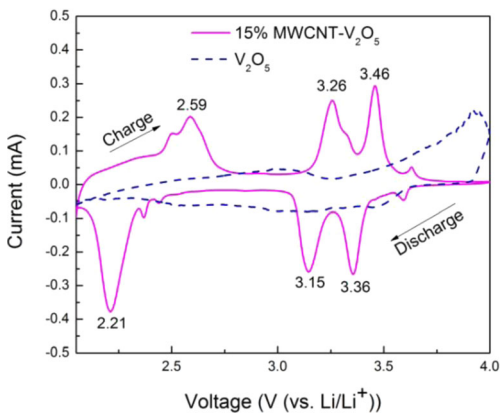

Fig. 5 Cyclic voltammetric curves of V_2O_5 powders and 15 % MWCNT–V_2O_5 nanocomposites at a scan rate of 0.1 mV s^{-1} in the voltage range between 2.05 and 4.0 V vs. Li/Li^+

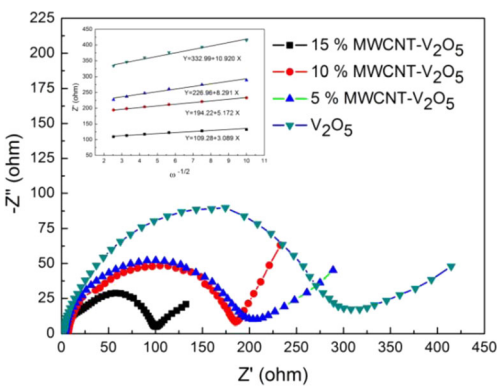

Fig. 6 Electrochemical impedance spectra of V_2O_5 powders and MWCNT–V_2O_5 nanocomposites at 3.4 V after 3 cycles. The *inset* shows the relationship curve between Z' and $\omega^{-1/2}$ in the low-frequency region

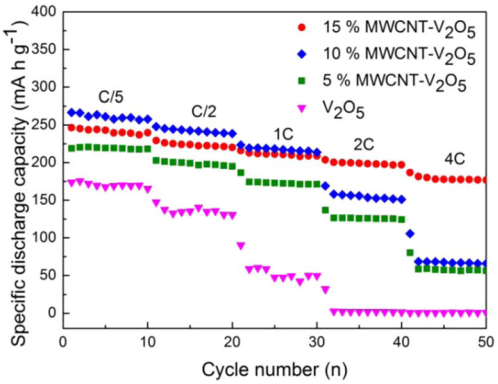

Fig. 7 Rate performance of V_2O_5 powders and MWCNT–V_2O_5 nanocomposites in the voltage range of 2.05 and 4.0 V vs. Li/Li^+. Here, 1 C=294 mA g^{-1}

depressed semicircles in the high-mediate frequency followed by a straight line in the low frequency. The high-frequency semicircle should be attributed to the contact resistance occurring because of the solid electrolyte interface (SEI) film, the medium-frequency semicircle is due to the charge transfer resistance at the electrode–electrolyte interface, and the slop line is related to the Li^+ diffusion process inside the electrode materials (Warburg resistance) [31–33]. The diameter of the medium-frequency semicircle corresponds to the charge transfer resistance (R_{ct}), and the charge transfer resistance for the 15 % MWCNT–V_2O_5 nanocomposite electrode is about 100 Ω, which is much less than that of 300 Ω for the V_2O_5 powder electrode. This result indicates that the charge transfer is much improved in MWCNT–V_2O_5 nanocomposite electrode, and it is a direct indication of the improved electrical conductivity arising from the intimate networking of MWCNTs with V_2O_5 nanoparticles which, in turn, facilitates a faster charge transfer between the V_2O_5 nanoparticles. Li^+ diffusion coefficient could be calculated from the low frequency plots according to the following Eqs. (1) and (2) [34, 35, 36]:

$$D_{\mathrm{Li}} = \frac{R^2T^2}{2n^4F^4S^2C^2\sigma^2} \tag{1}$$

where D_{Li} is the apparent diffusion coefficient, R is the gas constant, T is the absolute temperature, n is the number of electron transferred, F is the Faraday constant, S is the surface area of the electrode, C is the concentration of Li^+, and σ is the Warburg factor which is relative with Z',

$$Z' = R_{\mathrm{D}} + R_{\mathrm{L}} + \sigma\omega^{-1/2} \tag{2}$$

where ω is frequency, R_{D} is the charge transfer resistance, and R_{L} is the electrolyte resistance.

Based on the fitting linear equations in the inset of Fig. 6, Li^+ diffusion coefficients of pure V_2O_5 powders, 5, 10, and 15 % MWCNT–V_2O_5 nanocomposites are about 2.39×10^{-12}, 4.41×10^{-12}, 1.06×10^{-11}, and 2.98×10^{-11} cm^2 S^{-1}, respectively. Apparently, the addition of MWCNTs into bulk V_2O_5 is highly beneficial to Li^+ diffusion.

Figure 7 plots the rate capability of V_2O_5 powders and MWCNT–V_2O_5 nanocomposites at different rates. As shown in Fig. 7, the rate capability of MWCNT–V_2O_5 nanocomposites is greatly enhanced than that of V_2O_5 powders. The specific discharge capacity of V_2O_5 powder electrode at 0.2, 0.5, and 1 C is 176, 138, and 59 mA h g^{-1}, respectively (1 C= 294 mA g^{-1}), while that of 15 % MWCNT–V_2O_5 nanocomposite electrode increases to 245, 226, and 213 mA h g^{-1}, respectively. When the rate increased to 2 C (588 mA g^{-1}) and 4 C (1,176 mA g^{-1}), a specific discharge capacity of 200 and 180 mA h g^{-1} can be still retained for 15 % MWCNT–V_2O_5 nanocomposite electrode, but the capacity of V_2O_5 powder electrode can be almost ignored, only about 2 mA h g^{-1}. This observation demonstrates that the structure of the nanocomposites is very stable, and the electrochemical Li^+ insertion/extraction process is quite reversible. Ten percent MWCNT–V_2O_5 nanocomposite electrode delivers the specific discharge capacity of 261, 245, 220, 158, and 68 mA h g^{-1} at 0.2, 0.5, 1, 2, and 4 C, respectively. With regard to 5 % MWCNT–V_2O_5 nanocomposite electrode, the corresponding discharge capacity is 220, 201, 174, 126, and 58 mA h g^{-1}, respectively. It should be noted that the rate performance of 15 % MWCNT–V_2O_5 nanocomposites is much better in comparison with 10 and 5 % MWCNT–V_2O_5 nanocomposites and also better compared to other V_2O_5-based electrodes [9, 17] and possesses almost a similar rate capability to the V_2O_5/CTIT nanocomposite [21], but the synthesis of the V_2O_5/CTIT structure is much more complicated.

Conclusions

MWCNT–V_2O_5 nanocomposites have been synthesized using a facile and environmental friendly hydrothermal method without any pretreatment, surfactants, or chelate agents added. Compared to synthesized pure V_2O_5 powders, the MWCNT–V_2O_5 nanocomposites exhibit enhanced electrochemical performance as a cathode material for LIBs. The superior electrochemical performance of the nanocomposites is attributed to the fact that the electronically conducting networks and large surface areas were developed from the MWCNTs, which facilitate fast transportation and intercalation kinetics of Li ions. Furthermore, the method developed in this study opens up a new prospect for facile synthesis of hybrid nanomaterials for LIBs.

Acknowledgments This work is partly supported by the National Natural Science Foundation of China (grant no. 51202297), Program for New Century Excellent Talents in University (NCET-12-0554), the National Basic Research Program of China (973 Program) (grant no. 2013CB932901), the Creative Research Group of the National Natural Science Foundation of China (no. 50721003), and the Fundamental Research Funds for the Central Universities of Central South University (2013zzts019).

References

1. Tarascon JM, Armand M (2001) Nature 414:359–367
2. Scrosati B, Garche J (2010) J Power Sources 195:2419–1430
3. Wang Y, Cao G (2006) Chem Mater 18:2787–1800
4. McGraw JM, Bahn CS, Parilla PA, Perkins JD, Readey DW, Ginley DS (1999) Electrochim Acta 45:187–196
5. Wang Y, Takahashi K, Lee K, Cao G (2006) Adv Funct Mater 16: 1133–1144
6. Wang Y, Cao G (2008) Adv Mater 20:2251–2269
7. Takahashi K, Limmer SJ, Wang Y, Cao G (2004) J Phys Chem B 108(28):9795–9800
8. Pan A, Zhang JG, Nie Z, Cao G, Arey BW, Li G, Liang S, Liu J (2010) J Mater Chem 20:9193–9199
9. Cheah YL, Gupta N, Pramana SS, Aravindan V, Wee G, Srinivasan M (2011) J Power Sources 196:6465–6472
10. Ponzio EA, Benedetti TM, Torresi RM (2007) Electrochim Acta 52: 4419–4427
11. Li G, Pang S, Jiang L, Guo Z, Zhang Z (2006) J Phys Chem B 110: 9383–9386
12. Wang Y, Zhang HJ, Siah KW, Wong CC, Lin J, Borgna A (2011) J Mater Chem 21:10336–10341
13. Zhou F, Zhao X, Liu Y, Yuan C, Li L (2008) Eur J Inorg Chem 2506-2509
14. Wang Y, Takahashi K, Shang H, Cao G (2005) J Phys Chem B 109(8):3085–3088
15. Wang S, Li S, Sun Y, Feng X, Chen C (2011) Energy Environ Sci 4: 2854–2857
16. Pan A, Wu HB, Yu L, Zhu T, Lou XW (2012) Appl Mater Interfaces 4:3874–3879
17. Wang S, Lu Z, Wang D, Li C, Chen C, Yin Y (2011) J Mater Chem 21:6365–6369
18. Liu XM, Huang ZD, Oh S, Ma PC, Chan PCH, Vedam GK, Kang K, Kim JK (2010) J Power Sources 195:4290–4296
19. Sakamoto JS, Dunn B (2002) J Electrochem Soc 149:A26–30
20. Sathiya M, Prakash AS, Ramesha K, Tarascon JM, Shukla AK (2011) J Am Chem Soc 133:16291–16299
21. Hu YS, Liu X, Muller JO, Schlogl R, Maier J, Su DS (2009) Angew Chem Int Ed 48:210–214
22. Seng KH, Liu J, Guo ZP, Chen ZX, Jia D, Liu HK (2010) Electrochem Commun 13:383–386
23. Chen X, Zhu H, Chen YC, Shang Y, Cao A, Hu L, Rubloff GW (2012) ACS Nano 9:7948–7955
24. Cao Z, Wei B (2013) Nano Energy 2:481–490
25. Cava RJ, Santoro A, Murphy DW, Zahurak SM, Fleming RM, Marsh P, Roth RS (1986) J Solid State Chem 65:63–71
26. Ng SH, Patey TJ, Büchel R, Krumeich F, Wang JZ, Liu HK, Pratsinis SE, Novák P (2009) Phys Chem Chem Phys 11: 3748–3755
27. Braithwaite JS, Catlow CRA, Gale JD, Harding JH, Ngoepe PE (2000) J Mater Chem 10:239–240
28. Odani A, Pol VG, Pol SV, Koltypin M, Gedanken A, Aurbach D (2006) Adv Mater 18:1431–1436
29. Rui XH, Ding N, Liu J, Li C, Chen CH (2010) Electrochim Acta 55: 2384–2390
30. Wang ZL, Xu D, Wang LM, Zhang XB (2012) ChemPlusChem 77: 124–128
31. Nobili F, Croce F, Scrosati B, Marassi R (2001) Chem Mater 13: 1642–1646
32. Kang YJ, Kim JH, Lee SW, Sun YK (2005) Electrochem Acta 50: 4784–4791
33. Shenouda AY, Liu HK (2008) J Power Sources 185:1386–1391
34. Rho YH, Kanamura K (2004) J Solid State Chem 177:2094–2100
35. Liu S, Zhang J, Huang K, Yu J (2008) J Braz Chem Soc 19:1078–1083
36. Wang H, Huang K, Ren Y, Huang X, Liu S, Wang W (2011) J Power Sources 196:9786–9791